



Revisiting acetoclastic methanogens in anaerobic digestion via r/K selection-informed mathematical modeling

Title	Revisiting acetoclastic methanogens in anaerobic digestion via r/K selection-informed mathematical modeling
Author(s)	Chang, Huanhuan;Liu, Tingxia;Desmond-Le Quéméner, Elie;Ranjbar, Samira;Wu, Guangxue
Publication Date	2025-10-18
Publisher	Elsevier
Repository DOI	https://doi.org/10.1016/j.jwpe.2025.108884

1 **This paper has been published as**

2

3 **Huanhuan Chang, Tingxia Liu, Elie Desmond-Le Quéméner, Samira Ranjbar, *Guangxue***

4 ***Wu*. Revisiting acetoclastic methanogens in anaerobic digestion via r/K selection-informed**

5 **mathematical modelling. *Journal of Water Process Technology*, 2025, 79: 108884.**

6 **<https://doi.org/10.1016/j.jwpe.2025.108884>**

7 **Revisiting acetoclastic methanogens in anaerobic digestion via r/K selection-informed**
8 **mathematical modeling**

9

10 **Huanhuan Chang^a, Tingxia Liu^a, Elie Desmond-Le Quéméner^b, Samira Ranjbar^a,**
11 **Guangxue Wu^{a,*}**

12

13 ^aCivil Engineering, School of Engineering, College of Science and Engineering, University of
14 Galway, Galway H91 TK33, Ireland

15 ^bINRAE, Univ Montpellier, LBE, 102 Avenue Des Etangs, 11100 Narbonne, France

16

17 *Corresponding author

18 E-mail: guangxue.wu@universityofgalway.ie

19 **Abstract**

20 Anaerobic digestion mathematical models (ADMMs) have been extensively employed for
21 simulating system performance and predicting microbial community dynamics. However,
22 accurately determining kinetic and stoichiometric parameters of specific microorganisms
23 remains a major challenge. To simulate the competitive dynamics between two types of
24 acetoclastic methanogens, *Methanosarcina* and *Methanothrix*, an ADMM incorporating the r/K
25 selection theory was developed. By integrating thermodynamic analysis with metabolic
26 pathway characterization, the kinetic parameters of the two methanogens were systematically
27 estimated. With calibration of the maintenance coefficient and the maximum biomass specific
28 electron-transfer rate, the thermodynamic energy dissipation approach provided a viable
29 framework for elucidating the distinct kinetic parameters of the two methanogens. Sensitivity
30 analysis revealed that biomass yield and acetate concentration strongly influenced
31 *Methanosarcina* enrichment during the long-time operation, whereas solids retention time (SRT)
32 was identified as the primary factor governing the enrichment of *Methanothrix*.
33 *Methanosarcina* exhibited a higher biomass yield under high organic concentration conditions,
34 whereas *Methanothrix* demonstrates a stable and sustained enrichment trend under extended
35 SRTs and low substrate concentrations. Moreover, continuous flow reactor (CFR) systems
36 exhibited a more pronounced microbial shift in response to acetate concentration variations.
37 The stable flow and reduced substrate fluctuations of CFR systems favored the enrichment of
38 *Methanothrix* over time.

39

40 **Keywords:** Anaerobic digestion mathematical model; Kinetic parameters; *Methanosarcina* and
41 *Methanothrix*; r-/K-strategists; Thermodynamic energy dissipation

42 **1. Introduction**

43 Anaerobic digestion (AD) is a widely applied biological process that decomposes organic
44 matter into biogas and plays a critical role in waste treatment and renewable energy production.
45 Among the key functional microorganisms in AD, methanogens are responsible for methane
46 generation. Particularly, acetoclastic methanogenesis, which converts acetate into methane,
47 contributes to over 60% of total methane output in most systems (Boone David et al., 1989;
48 Jetten et al., 1990; Pan et al., 2021). Notably, only two methanogens are known to perform this
49 function: *Methanosarcina* and *Methanotherix* (formerly *Methanosaeta*) (Duan et al., 2023).
50 These organisms differ significantly in their physiological characteristics and ecological
51 strategies (De Vrieze et al., 2012; Zhu et al., 2024). *Methanosarcina* is recognized as an r-
52 strategist, capable of rapid growth and thriving under high substrate concentrations and
53 dynamic conditions. In contrast, *Methanotherix* is a K-strategist with high substrate affinity, slow
54 growth, and a preference for stable environments (Aguilar-Muñoz et al., 2022; Yin et al., 2022).
55 Despite their importance, the mechanisms governing their coexistence, succession, and
56 competition remain underexplored. A critical knowledge gap exists in how environmental
57 parameters such as substrate concentration, operational modes, and solids retention time (SRT)
58 affect the selection and dominance of these two acetoclastic methanogens in engineered systems.

59
60 Anaerobic digestion mathematical models (ADMMS) have been extensively employed to
61 simulate AD processes (Batstone et al., 2002; Segura et al., 2025). Anaerobic digestion model
62 No. 1 (ADM1) provides a comprehensive framework that incorporates biochemical reactions,
63 microbial interactions, and environmental conditions (Mo et al., 2023). It enables the prediction
64 of system performance and the evaluation of microbial community dynamics (Batstone and
65 Keller, 2003; Couto et al., 2019; Silva et al., 2025). Using ADM1 to simulate the system
66 dynamics and microbial responses of AD under various operational conditions offers a faster

67 and more cost-effective alternative to experimental studies (Salma et al., 2025; Zhao et al.,
68 2019). However, despite its success, ADM1's application remains limited by the uncertainty
69 and variability in kinetic and stoichiometric parameters (Kleerebezem and van Loosdrecht,
70 2006; Mo et al., 2023), especially for less characterized microorganisms like *Methanothrix*.
71 Experimental determination of kinetic parameters is often time-consuming, condition-specific,
72 and prone to inaccuracies. For instance, values for maximum specific growth rates (μ_{\max}),
73 substrate affinity constants (K_s), and biomass yields (Y) vary significantly in literature,
74 sometimes by an order of magnitude (Conklin et al., 2006; Schmidt and Ahring, 1999; Wandrey
75 and Aivasidis, 1983). Furthermore, the lack of strain-specific data impedes the accurate
76 simulation of microbial competition and succession, particularly in dynamic systems such as
77 sequencing batch reactors (SBRs) and continuous-flow reactors (CFRs). The same ADM1-
78 recommended kinetic and stoichiometric parameters are widely used in AD models (Sani et al.,
79 2025; Sun et al., 2021a; Sun et al., 2021b), while *Methanosarcina* and *Methanothrix* differ
80 markedly in their parameter values when utilizing the same substrate. This gap highlights the
81 need for more systematic and theory-informed approaches to parameter estimation.

82

83 One promising strategy is to integrate thermodynamic principles into kinetic and stoichiometric
84 parameter estimation. Thermodynamic energy dissipation theory allows for the quantification
85 of kinetic parameters, such as microbial biomass yields, based on the amount of usable energy
86 extracted from catabolic reactions (Heijnen, 2002; Kleerebezem and Van Loosdrecht, 2010;
87 Wu et al., 2022). This method helps circumvent the limitations of purely empirical approaches
88 by grounding parameter estimation in biochemical reality (Heijnen and Van Dijken, 1992).
89 Previous studies have shown that thermodynamic modeling can offer reliable estimates for
90 energy-limited microbial systems (Delattre et al., 2020; Leurent and Moscoviz, 2022). The
91 Gibbs energy dissipation approach, which links microbial catabolism and anabolism through

92 energy losses, provides a robust framework for estimating growth parameters based on the
93 amount of biologically available energy. Given that *Methanosarcina* and *Methanotherix* differ
94 in their metabolic pathways and energy conversion, incorporating these differences into
95 thermodynamic calculations may allow for refined evaluation of their growth kinetics. Building
96 on this, we propose the integration of thermodynamic principles and metabolic energy into
97 ADMMs to enhance the mechanistic understanding and predictive accuracy of methanogenic
98 processes.

99

100 The r/K-strategist behavior of *Methanosarcina* and *Methanotherix* can be influenced by factors
101 such as substrate concentration, SRT, and reactor operation mode (e.g., CFRs and SBRs),
102 providing practical means to steer their dominance in acetoclastic methanogenesis. By
103 embedding r/K strategic traits within ADMM kinetic framework, the model enables simulation
104 of microbial succession and enrichment patterns driven by substrate availability and SRT (Liu
105 and Wu, 2023). This hybrid approach, combining energy-based parameter estimation and
106 ecological strategy modeling, offers a novel framework for enhancing the predictive accuracy
107 of AD models and guiding the design of robust, strategy-informed bioreactors.

108

109 In this study, a novel model framework that integrates r/K selection theory into anaerobic
110 digestion model was proposed, focusing on acetoclastic methanogens. The study aims to: (i)
111 derive the kinetic parameters of *Methanosarcina* and *Methanotherix* based on thermodynamic
112 energy dissipation principles, revisiting the thermo-kinetic approach proposed by Heijnen and
113 Van Dijken (1992); (ii) identify the key kinetic or stoichiometric parameters of the two
114 methanogens by sensitivity analysis; and (iii) investigate how reactor operational parameters
115 shape the competitive exclusion dynamics between r- and K-strategist in chemostat cultures.
116 Applying the r/K theory in ADMM can enhance our understanding of microbial ecology in AD

117 systems and support better system optimization for pollution control and energy production.

118

119 2. Materials and methods

120 2.1. Thermodynamic calculation

121 Corrected for temperature of the standard Gibbs energy can be obtained from the simplified
122 Gibbs-Helmholtz equation at non-standard temperatures (Kleerebezem and and Van Loosdrecht,
123 2010).

$$124 \quad G_f^0(T) = G_f^0(T_s) \times \frac{T}{T_s} + H_f^0(T_s) \times \frac{T_s - T}{T_s} \quad (1)$$

125 Where $G_f^0(T)$ and $G_f^0(T_s)$ is the Gibbs energy at actual temperature (T) and standard
126 temperature (T_s , 298.15 K), respectively. $H_f^0(T_s)$ is the enthalpy at T_s . Gibbs free energy was
127 calculated assuming liquid concentrations of 1 mol/L, gas partial pressures of 1 atm, pH of 7,
128 and temperature of 308.15 K.

129 Moreover, the actual Gibbs energy change (ΔG) reflecting the effect of substrate and product
130 concentrations, was calculated using the following equation:

$$131 \quad \Delta G = \Delta G^0 + RT \sum Y_i \ln c_i \quad (2)$$

132 where ΔG^0 is the Gibbs free energy change at 308.15 K, R is the gas constant (8.314
133 J/(K·mol)), Y_i represents the stoichiometric coefficient of compound i , c_i is the concentration
134 of compound i .

135 Table S1 presents the Gibbs energy values of key reactions in acetate oxidation. Although the
136 chemical reaction ($\text{CH}_3\text{COO}^- + \text{H}^+ \rightarrow \text{CH}_4 + \text{CO}_2$) is traditionally used to represent the catabolic
137 conversion of acetate to methane, it fails to capture the energetic differences between
138 *Methanosarcina* and *Methanotherix* (Jin, 2012; Welte and Deppenmeier, 2014; Wu et al., 2022).
139 Despite catalyzing the same overall reaction, these two methanogens exhibit distinct ATP yields

140 due to differences in their metabolic pathways (Jin, 2012; Welte and Deppenmeier, 2014).
 141 Therefore, this study adopts an ATP-based quantification approach to more accurately
 142 characterize the energy generation associated with their catabolic metabolism (ΔG_{cat}) (Jin, 2012;
 143 Patón and Rodríguez, 2019). The same anabolism energy (ΔG_{an}) is applied for both
 144 *Methanosarcina* and *Methanotherix*.

145

146 Since only part of the catabolic energy supports microbial growth, the remaining portion,
 147 defined as dissipated energy, is estimated using Eq. (3) (Heijnen and Kleerebezem, 2010).

$$148 \quad \Delta G_{\text{dis}} = 200 + 18 \cdot (6 - \text{NoC})^{1.8} + \exp \left[\left\{ (3.8 - \gamma)^2 \right\}^{0.16} \cdot (3.6 + 0.4 \cdot \text{NoC}) \right] \quad (3)$$

149 Here, NoC represents the number of carbon atoms in the carbon source, and γ refers to the
 150 degree of reduction of the carbon source (e^- per C-mol of organic or per mol inorganic carbon).
 151 For acetate, NoC is 2 and γ is 4. The stand Gibbs dissipation energy for acetate degradation is
 152 -432 kJ/C-mol biomass. Then, the catabolic multiplication factor (λ), which represents the
 153 number of times the catabolic reaction must proceed to generate sufficient Gibbs free energy
 154 for the synthesis of one C-mol of biomass, can be estimated using the dissipation energy
 155 approach (Kleerebezem and and Van Loosdrecht, 2010).

$$156 \quad \lambda = \frac{\Delta G_{\text{an}} + \Delta G_{\text{dis}}}{-\Delta G_{\text{cat}}} \quad (4)$$

157 Finally, The biomass yield coefficient, decay coefficient (k_d), maximum biomass specific
 158 electron-transfer rate (q_e^{max}), the maximal rate of Gibbs energy (q_G^{max}), Gibbs energy
 159 requirements for maintenance (m_G), and μ_{max} were calculated based on thermodynamics
 160 analysis (see Supplementary Material 1) (Heijnen and Kleerebezem, 2010; Heijnen and Van
 161 Dijken, 1992; Tijhuis et al., 1993).

162

163 **2.2. Model establishment and simulation**

164 The anaerobic acetate degradation was simulated using the AQUASIM 2.0 software (Reichert,
165 1994, 1998). In the models, *Methanosarcina* and *Methanothrix* were regard as r- and K-
166 strategists, respectively. Each microbial group was initialized at a biomass concentration of 3 g
167 COD/L. The total bioreactor volume was 6 L, with 5 L working liquid and 1 L headspace. The
168 system operated at the temperature of 35°C with hydraulic retention time of 24 h. For SBR
169 configuration, the feed phase was set to a duration of 0.03 d. Additionally, the gas-liquid transfer
170 of H₂, CO₂, and CH₄ was also simulated. The mass transfer rate is represented by Eq. (5):

$$171 \quad P_{T,i} = K_L a (S_{liq,i} - K_{H,i} P_{gas,i}) \quad (5)$$

172 Where $P_{T,i}$ (M/d) represents the mass transfer rate of the gas component i , and $K_L a$ (1/d) is the
173 volumetric gas-liquid mass transfer values. A uniform $K_L a$ value for CO₂, H₂, and CH₄ is applied
174 as suggested in ADM1 (Batstone et al., 2002), with the value of 3.2 1/d (Merkel and Krauth,
175 1999). $S_{liq,i}$ (M) is the concentration of component i in the liquid phase; $K_{H,i}$ (M/bar) is Henry's
176 constant of component i ; $P_{gas,i}$ (bar) represents the partial pressure of component i in the gas
177 phase. The headspace pressure was assumed to be 1 atm, and all gases were considered to follow
178 the ideal gas law (Batstone et al., 2002). Details regarding the implemented processes, reaction
179 kinetics, and model parameters in the developed ADMM are provided in Table S2 - S3.

180

181 The kinetic and stoichiometric parameters incorporated into the model were obtained from
182 multiple sources (Table S4): thermodynamic calculations in this study, experiment and model
183 data reported in earlier studies, traditional ADM1, and literature-based average values specific
184 to *Methanosarcina* and *Methanothrix*. All models were simulated until they reached a stable
185 state; otherwise, results were taken after 4000 days of operation. The minimum concentration
186 for all compounds was set at 10⁻⁶ g COD/L.

187

188 **2.3. Sensitivity analysis**

189 To assess the key factors (operational conditions, kinetic, and stoichiometric parameters)
190 influencing the selection of r- and K-strategists, a sensitivity analysis was performed.
191 Considering the variation among different datasets, using the literature-based average values is
192 reasonable in sensitivity analysis. The sensitivity index (SI) is defined by Eq. (6) (Reichert,
193 1994):

$$194 \quad SI = \delta_{y,p}^{a,r} = p \frac{\delta y}{\delta p} \quad (6)$$

195 Where $\delta_{y,p}^{a,r}$ refers to the absolute-relative sensitivity function, y denotes the state variable, and
196 p represents the parameters analyzed. A positive sensitivity index value indicates a positive
197 relationship between parameter p and state variable y , whereas a negative SI suggests an inverse
198 relationship. In this analysis, the microbial concentrations of *Methanosarcina* and *Methanothrix*
199 were selected as the state variables to evaluate parameter sensitivity.

200

201 **2.4. Effects of SRT and acetate concentration on the selection of *Methanosarcina* and** 202 ***Methanothrix***

203 The developed model with literature-based average kinetic and stoichiometric values was used
204 to simulate two sets of scenarios under both SBR and CFR: SRTs varying from 5 to 200 days
205 with acetate maintained at 3 g COD/L, and acetate concentrations ranging from 0.2 to 15 g
206 COD/L under a fixed SRT of 25 days.

207

208 3. Results and discussion

209 3.1. Literature survey of kinetic and stoichiometric parameters for *Methanosarcina* and 210 *Methanotherix*

211 Fig. 1 presents a comparison of key kinetic and stoichiometric parameters between
212 *Methanosarcina* and *Methanotherix* based on literature data (Supplementary material 1),
213 revealing distinct ecological strategies aligned with r-/K-strategists (Andrews and Harris, 1986;
214 Yin et al., 2022). *Methanosarcina* shows a higher average biomass yield of 0.055 g COD
215 biomass/g COD acetate, compared to 0.032 g COD biomass/g COD acetate for *Methanotherix*.
216 Similarly, μ_{\max} of *Methanosarcina* averages 0.60 1/d, nearly three times of *Methanotherix* (0.22
217 1/d), with *Methanosarcina* also showing higher inter-study variability. The half-saturation
218 constant for *Methanosarcina* is significantly higher at 265.9 mg COD/L, indicating a lower
219 substrate affinity than *Methanotherix*, which has an average K_S of 57.7 mg COD/L. The
220 maximum specific substrate utilization rate (k_m) of *Methanosarcina* is 9.02 g COD acetate/g
221 COD biomass/d, while *Methanotherix* averages only 2.95 g COD acetate/g COD biomass/d.
222 Notably, the decay rate (k_d) for *Methanosarcina* is 0.055 1/d, which is more than five times
223 higher than *Methanotherix* at 0.01 1/d, suggesting a higher maintenance energy requirement and
224 turnover rate of *Methanosarcina* (Conklin et al., 2006).

225
226 These differences reinforce the classification of *Methanosarcina* as an r-strategist, whereas
227 *Methanotherix* behaves as a K-strategist, adapted to stable environments with lower substrate
228 levels (De Vrieze et al., 2012; Zhu et al., 2024). Moreover, *Methanotherix* exhibits lower kinetic
229 parameter values with tighter interquartile ranges, indicative of a more specialized, K-strategist
230 lifestyle optimized for efficiency and persistence under stable conditions. *Methanosarcina*
231 exhibits a much wider distribution in its K_S , ranging from 140 to nearly 365 mg COD/L,
232 indicating substantial variability across studies (interquartile range spans over 200 mg/L). In

233 contrast, *Methanothrix* shows a tighter distribution around its average of 57.71 mg COD/L,
234 suggesting more consistent affinity characteristics. Similarly, k_a of *Methanosarcina* also shows
235 high dispersion, with values ranging from near 0 to 0.1 1/d, while *Methanothrix* displays
236 minimal spread around its much lower average of 0.01 1/d. This greater variability in
237 *Methanosarcina*'s parameters could reflect its metabolic flexibility and broader adaptability
238 under diverse environmental conditions, consistent with r-strategist behavior (De Vrieze et al.,
239 2012).

240

241 **3.2. Thermodynamic calculation**

242 The thermodynamic energy dissipation approach was employed to estimate the kinetic
243 parameters of *Methanosarcina* and *Methanothrix*. The energy generated during their catabolic
244 metabolism was assessed based on ATP yield via their metabolic pathways. It is commonly
245 assumed that *Methanosarcina* yields approximately 0.75 mol ATP per mol acetate, while
246 *Methanothrix* produces around 0.25 mol ATP per mol acetate, due to differences in their energy
247 conservation pathways (Jin, 2012). Assuming a standard Gibbs free energy of ATP hydrolysis
248 of 60 kJ/mol, the catabolic energy yields of *Methanosarcina* and *Methanothrix* are estimated to
249 be approximately -45 kJ/mol and -15 kJ/mol, respectively, under standard conditions. These
250 estimates are context-dependent and influenced by factors such as electron transport chain
251 architecture and chemiosmotic efficiency (Buan, 2018). While exact ATP yields may vary with
252 environmental conditions, the values are cited here to reflect general trends in their metabolic
253 energetics. Then the dissipated catabolic energy was calculated and subsequently used to
254 determine Y via the thermodynamic model. However, when calculating the maintenance energy
255 and decay coefficient using conventional thermodynamic approaches, the resulting values were
256 unrealistically high and required correction (Bonk et al., 2019) (Table S5). To address this, a
257 maintenance energy value of $m_D = 0.003$ mol acetate/mol biomass/h was adopted for

258 *Methanosarcina* (Wandrey and Aivasidis, 1983), while *Methanothrix* was assumed to require
259 half of that value. Based on these assumptions, the corresponding values of Gibbs maintenance
260 energy were then derived. It is important to note that the q_e^{\max} , corresponds to the parameter k_m
261 in ADMM, is determined solely by temperature and substrate properties in thermodynamic
262 approaches. The calculated value of 308 K (7.31 mol e⁻/mol biomass/h) was significantly higher
263 than expected, and with no difference in *Methanosarcina* and *Methanothrix* (Table S5) (Heijnen
264 and Kleerebezem, 2010). Therefore, the literature-based average values of k_m were adopted for
265 correction, yielding q_e^{\max} values of 1.58 mol e⁻/mol biomass/h for *Methanosarcina* and 0.52
266 mol e⁻/mol biomass/h for *Methanothrix* (Table S5).

267

268 The trends observed in Y and μ_{\max} with varying catabolic energy (represents varying energy
269 utilization efficiencies 10% ~ 100%) are depicted in Fig. 2, highlighting the sensitivity of these
270 kinetic and stoichiometric parameters to underlying thermodynamic assumptions. The
271 thermodynamic analysis clearly demonstrated that Y of *Methanosarcina* and *Methanothrix*
272 increased linearly with the decrease in Gibbs free energy change (ΔG_{cat}), indicating a direct
273 relationship between available energy and microbial biomass yield. The variation in μ_{\max} was
274 slight in this study, as μ_{\max} was associated with q_G^{\max} , which was held constant. For
275 *Methanosarcina*, as ΔG_{cat} becomes more negative from -4.65 to -46.49 kJ/mol acetate, Y rised
276 from 0.005 to 0.049 g COD biomass/g COD acetate, with the μ_{\max} of 0.49 1/d. For *Methanothrix*,
277 Y increased from 0.002 to 0.017 g COD biomass/g COD acetate across ΔG_{cat} values of -1.55 to
278 -15.5 kJ/mol acetate, with the μ_{\max} of 0.052 1/d. The calculated results revealed that the μ_{\max} of
279 *Methanothrix* is significantly lower than experimentally reported values. This discrepancy may
280 be attributed to underestimation of catabolic energy release or overestimation the energy
281 dissipation of *Methanothrix* (Heijnen and Kleerebezem, 2010), suggesting that the metabolic
282 pathway could be more efficient (Buan, 2018). Patón and Rodríguez (2019) suggested that

283 model calibrations could target μ_{\max} with maintaining the upper bioenergetic limit of microbial
284 growth yield. Moreover, *Methanothrix*, with a higher energy utilization efficiency, can persist
285 at much lower ΔG_{cat} values, potentially explaining its dominance under low-acetate conditions.
286 Due to the absence of a reliable estimation approach for the half saturation constant (Heijnen
287 and Kleerebezem, 2010), its value was adopted from the literature-based average value in the
288 subsequent modeling.

289

290 These results indicate that while thermodynamic-based approaches can provide reasonable
291 estimates of parameters estimation for *Methanosarcina*, their applicability to *Methanothrix*
292 appears limited. However, the results also indicated that the thermodynamic energy dissipation
293 approach is a promising method for differentiating microbial kinetic parameters for
294 *Methanosarcina* and *Methanothrix* (Heijnen and Kleerebezem, 2010; Picioreanu et al., 2007).
295 Based on biomass yield values reported in the literature, the Gibbs energy dissipation was
296 estimated to be approximately 389.1 kJ/mol for *Methanosarcina* and 215.8 kJ/mol for
297 *Methanothrix*, highlighting a substantial difference in energy dissipation between the two
298 organisms. These calculated values are in line with previous findings suggesting that rapid
299 microbial growth is often associated with increased energy dissipation, as fast-growing cells
300 require higher metabolic fluxes (Heijnen and Van Dijken, 1992; von Stockar, 2014). These
301 estimations, however, should be interpreted with caution and warrant further validation. This
302 underscores the importance of refining parameters, such as ΔG_{dis} in a strategy-specific manner
303 in future modeling studies (Heijnen and Kleerebezem, 2010; Wu et al., 2022). as *Methanothrix*
304 may dissipate less energy than *Methanosarcina*, enabling its survival under more energy-limited
305 conditions. Moreover, recent study showed that *Methanosarcina* exhibits a significantly higher
306 energy threshold (19.7 ± 2.7 kJ/mol) compared to *Methanothrix* (11.8 ± 5.2 kJ/mol) (Jin,
307 2012), suggesting a greater minimum free energy requirement for initiating metabolism. This

308 difference supports the interpretation that *Methanothrix*, with its lower energy threshold, is
309 better adapted to persist in energy-limited environments where substrate concentrations are low.
310

311 **3.3. Simulation results based on different data sources**

312 A detailed comparison of the simulation results based on five data sources (Table S4) revealed
313 the biomass dynamics patterns of *Methanosarcina* (r-strategist) and *Methanothrix* (K-strategist),
314 shaped by their physiological traits and model parameters (Fig. 3). In all simulations, a
315 standardized condition was applied with an SRT of 25 days and an influent acetate
316 concentration of 3 g COD/L.

317

318 In all scenarios, as the system stabilizes, *Methanosarcina* outcompetes *Methanothrix* in both
319 SBR and CFR. It was suggested that under the given operational conditions (SRT = 25 d, acetate
320 = 3 g COD/L), r-strategists are better adapted to long-term steady-state environments,
321 ultimately leading to their dominance. Particularly striking is the thermodynamic-based model,
322 *Methanosarcina* consistently dominates over *Methanothrix* throughout the entire operation
323 period in both SBR and CFR systems. It might be attributed to that *Methanothrix* exhibits a
324 much lower biomass yield ($Y = 0.017$ g COD biomass/g COD acetate) than *Methanosarcina*
325 ($Y = 0.049$ g COD biomass/g COD acetate), limiting its biomass accumulation. The
326 thermodynamic-based parameters might underestimate the competitive edge of K-strategists
327 under these conditions, leading to the persistent suppression of K-strategists. Based on the
328 datasets from the experiment of Conklin et al. (2006) and the model of Figdore et al. (2013), at
329 the early stage of operation, *Methanothrix* exhibits higher biomass concentrations in both SBR
330 and CFR systems, probably benefiting from its high substrate affinity and efficient substrate
331 utilization. However, as time progresses, *Methanosarcina* gradually increases and surpasses
332 *Methanothrix* at the steady-state phase. This shift may be attributed to *Methanosarcina*'s higher

333 maximum specific growth rate. In [Conklin et al. \(2006\)](#) dataset, a longer time is required to
334 reach steady-state conditions compared to [Figdore et al. \(2013\)](#). This is likely due to the
335 relatively high decay coefficient for both *Methanosarcina* (0.098 1/d) and *Methanothrix* (0.006
336 1/d) ([Conklin et al., 2006](#)). A higher decay rate leads to faster biomass loss, especially in the
337 initial phase, thereby prolonging the time needed for biomass to stabilize. The ADM1
338 recommends low decay rates (0.01 ~ 0.02 1/d), but due to the strong correlation between decay
339 and uptake rates, higher decay rates, as used in the [Siegrist et al. \(2002\)](#) model (0.05 1/d), can
340 be offset by increased uptake rates.

341

342 In contrast to datasets derived from specific experimental studies or thermodynamic
343 considerations, the traditional ADM1 model does not differentiate *Methanosarcina* and
344 *Methanothrix*, treating methanogens as a mixed population with uniform kinetic parameters
345 ([Batstone et al., 2002](#)). As a result, the simulated biomass yields concentration is slightly higher
346 in the SBR system compared to CFR. This suggests that the operational mode of SBR,
347 characterized by high concentrations immediately after feeding, is more favorable for
348 *Methanosarcina*, which thrives under fluctuating and high-acetate environments, in contrast to
349 the more constant and diluted conditions in CFR.

350

351 The concentration profiles of acetate, CH₄, along with the Gibbs free energy change in SBR
352 and CFR systems based on model simulations using literature-based average values are shown
353 in [Fig. S1](#). In SBR system, acetate concentrations exhibited periodic fluctuations due to batch
354 feeding and were rapidly depleted (< 4 h), accompanied by corresponding decreases in available
355 energy (-40 to -3 kJ/mol) during consumption. In contrast, the CFR system maintained stable
356 acetate levels (~ 0.1 g COD/L) and consistently favorable ΔG values (-32 kJ/mol). The
357 thermodynamically favorable conditions ($\Delta G < -30$ kJ/mol) in both systems supported the

358 dominance of *Methanosarcina*, which grows faster than *Methanothrix* at 3 g COD/L under 25
359 days SRT. Overall, *Methanosarcina* exhibited higher biomass concentrations, despite
360 *Methanothrix*'s low decay rate and substrate threshold, its biomass accumulation remains
361 minimal due to the low growth yield. These findings support the niche differentiation theory,
362 highlighting *Methanosarcina*'s preference for fluctuating, nutrient-rich conditions.

363

364 **3.4. Sensitivity analysis**

365 To evaluate the influence of key parameters on model performance, a dynamic sensitivity
366 analysis was conducted. The sensitivity index was calculated over a simulation period of 200
367 days for six representative kinetic and operational parameters: k_m , K_S , k_d , SRT, Y , and acetate
368 concentration (AC) (Fig. 4).

369

370 For *Methanosarcina* in SBR, as illustrated in Fig. 4a, Y and AC exhibited the highest sensitivity
371 indices throughout the simulation, both stabilizing above 1.0 after approximately 50 days. This
372 suggests that biomass yield efficiency and acetate concentration are the most influential
373 variables governing acetate degradation under r-strategist selection conditions. SRT
374 demonstrated a unique time-dependent sensitivity pattern. During the initial phase (0 ~ 14 days),
375 SRT showed an increase SI exceeding 0.5, suggesting that extending the SRT significantly
376 enhanced system stability and biomass retention in early development. However, the SI of SRT
377 gradually declined (14 ~ 75 days) and fluctuated at lower levels, indicating a reduced influence
378 in the later phase. It then gradually increased again and eventually stabilized at around 0.46
379 during the steady-state phase. This dynamic highlights the importance of carefully controlling
380 SRT during the start-up period of r-strategist dominated systems to support rapid growth, while
381 excessive retention in the steady state may offer diminishing returns.

382

383 Notably, k_d showed a pronounced negative SI in the initial phase (down to -0.93 at day 20),
384 indicating that increased cell decay adversely affected system performance during start-up (Liu
385 and Wu, 2023). Over time, this impact diminished to -0.69 as the microbial population adapted
386 to operational conditions. k_m showed moderate sensitivity (SI peaking at 0.54), particularly
387 during the early operational phase (0 ~ 50 days), indicating that growth kinetics of r-strategists
388 are critical during the initial colonization and acclimation (Chen et al., 2016). In contrast, K_S
389 exhibited consistently low sensitivity. Havlik et al. (1984) also found that yield coefficients and
390 rate constants were the most influential parameters in anaerobic digestion modeling, while
391 saturation constants had minimal impact. A similar SI trend of *Methaosarcina* was observed in
392 CFR (Fig. 4b), except that the SI of SRT became negative between days 30 and 95, indicating
393 that extended SRT during this period may have limited biomass growth of r-strategist (López
394 and Borzacconi, 2010; Melcer, 2004). In contrast, K_S in the CFR system demonstrated a more
395 pronounced negative sensitivity, especially around day 50, suggesting that substrate affinity
396 played a more influential role in the continuous system.

397

398 For *Methanothrix* in SBR (Fig. 4c), SRT exhibited the highest influence, reaching a peak SI
399 value exceeding 1.0 at day 20 to 40, indicating its critical role during the early operational phase.
400 k_m and Y showed moderate sensitivity, peaking between 32 to 65 days and gradually declining
401 afterward. In contrast, k_d maintained a consistently negative SI, highlighting its persistent
402 adverse effect on system behavior. Notably, K_S remained near zero throughout the simulation
403 period, suggesting minimal influence on the system's response and indicating potential for
404 model simplification. AC showed a transient slight impact, with its SI peaking (0.19) in the
405 early phase before declining, implying a limited but time-specific role.

406

407 For *Methanothrix* in the CFR configuration (Fig. 4d), a similar trend of sensitivity indices was

408 observed of SRT, Y , and k_m , except that they reached slightly higher peak values compared to
409 those in the SBR system. Consistent with the trend observed for *Methanosarcina*, K_s in the
410 CFR system exhibited a more pronounced influence on *Methanothrix* compared to the SBR
411 system. The sensitivity index for k_d reached a deeper negative value and persisted longer for
412 *Methanothrix* in SBR compared to CFR. This suggests that biomass loss due to endogenous
413 decay of *Methanothrix* is more detrimental in the SBR system, possibly due to the periodic
414 discontinuities in feeding that reduce resilience to decay-driven biomass reduction. In the CFR
415 system, the continuous inflow may help maintain a more stable microbial population for K-
416 strategists, mitigating the impact of endogenous decay (Conklin et al., 2006).

417

418 This analysis provides quantitative guidance for parameter prioritization during model
419 calibration and system design. Particularly, it emphasizes the importance of optimizing Y and
420 AC for *Methanosarcina*, especially in the early phase, for enhanced anaerobic acetate
421 degradation performance. For *Methanothrix*, with proper SRT control in the early stage, the
422 system naturally transitions into a stable state. Given that the kinetic parameters cannot be
423 directly manipulated in practice, operational variables such as SRT and acetate concentration
424 were used as key levers to achieve the desired system dynamics.

425

426 **3.5. Effect of SRT on the selection of r-/K-strategists**

427 SRT is a key parameter in bioreactor operation, since insufficient retention time may result in
428 microbial washout (Rittmann and McCarty, 2020). This study investigated the biomass
429 distribution patterns of *Methanosarcina* and *Methanothrix* under varying SRTs using the
430 average of the surveyed kinetic data. To enable a comprehensive analysis, four acetate
431 concentrations were selected: 0.2, 0.75, 3, and 5 g COD/L (Fig. 5). The results demonstrated
432 that SRT significantly influenced the competition between these two acetoclastic methanogens.

433

434 In the SBR system, under low acetate concentration (0.2 g COD/L), the biomass of
435 *Methanothrix* continuously increased with prolonged SRT, eventually outcompeting
436 *Methanosarcina* at an SRT of 30 days. In contrast, *Methanosarcina* showed a slight high
437 accumulation than *Methanothrix* at low SRT (< 30 days), followed by a decline, indicating that
438 long SRT was unfavorable for its persistence at low acetate concentration (Chang et al., 2024;
439 Lv et al., 2016). At a moderate acetate concentration (0.75 g COD/L), *Methanosarcina*
440 exhibited rapid early growth and dominant when SRT < 70 days, and its biomass also gradually
441 declined at higher SRTs. Meanwhile, *Methanothrix* slowly accumulated and eventually
442 surpassed *Methanosarcina* at approximately 70 days of SRT, indicating that longer SRTs favor
443 the later enrichment of *Methanothrix*. Under higher acetate concentration (3 g COD/L),
444 *Methanosarcina* maintained a high biomass across the SRT range, peaking at around 1.76 g
445 COD/L at 150 days SRT. Although *Methanothrix* grew more slowly, it gradually caught up and
446 approached the biomass level of *Methanosarcina* after SRT > 180 day. This indicates that while
447 *Methanosarcina* is more adaptive to high substrate conditions, *Methanothrix* can also enrich
448 under extended SRTs. At the highest acetate concentration (5 g COD/L), *Methanosarcina*
449 clearly dominated. *Methanothrix* remained at a lower biomass level than *Methanosarcina*
450 during the entire period (SRT < 250 days), until *Methanothrix* eventually gained dominance at
451 an SRT of 280 days. Overall, these results suggest that *Methanothrix* holds a competitive
452 advantage under low substrate concentrations and extended SRTs, whereas *Methanosarcina*
453 gains a competitive edge under high substrate loads and short SRTs (Conklin et al., 2006; De
454 Vrieze et al., 2012; Lee et al., 2025). This reflected distinct ecological niches and physiological
455 strategies, offering valuable guidance for regulating acetoclastic methanogenesis in anaerobic
456 digestion systems.

457

458 In the CFR system, under low organic concentrations (0.2 and 0.75 g COD/L), *Methanosarcina*
459 dominated during the early stages, with significantly higher biomass than *Methanothrix* at short
460 SRTs (< 50 days). Under high organic concentrations (3 and 5 g COD/L), *Methanosarcina* also
461 exhibited early dominance, peaking at 2.7 g COD/L at an SRT of 45 days under 5 g COD/L
462 conditions. However, *Methanothrix* showed a late-stage bloom, surpassing *Methanosarcina* at
463 55 days SRT. Notably, under 5 g COD/L conditions, *Methanothrix* reached a biomass of 3.5 g
464 COD/L at 55 days SRT, while *Methanosarcina* declined sharply to only 0.01 g COD/L.
465 Although *Methanothrix* was also able to accumulate in the CFR under a low organic
466 concentration (0.2 g COD/L), its biomass remained lower than in the SBR system. Under high
467 acetate concentrations (e.g., 3 and 5 g COD/L), *Methanothrix* overtook *Methanosarcina* at
468 lower SRTs in the CFR compared to the SBR. This implies that the continuous operation of
469 CFR enhanced the competitive advantage of *Methanothrix*, probably due to its higher acetate
470 affinity and better adaptation to stable environments (Chang et al., 2024). In contrast,
471 *Methanosarcina* showed some degree of resilience to increasing SRT in the SBR, while in the
472 CFR (Fig. 5c, d), it was completely disappeared once SRT exceeded 55 days. The intermittent
473 feeding capability of the SBR allowed *Methanosarcina* to maintain dominance for a longer
474 duration (Chang et al., 2024). Therefore, in engineering applications aimed at enriching
475 *Methanosarcina*, the SBR may be the more favorable reactor type (Chang et al., 2025). An
476 interesting phenomenon was observed that *Methanothrix* was able to persist for extended
477 periods even below its critical SRT. For instance, it remained detectable in SBRs at 3 g COD/L
478 with an SRT of 180 days and at 5 g COD/L with an SRT 270 days, as well as in CFRs at 3 g
479 COD/L and 5 g COD/L with 50 days SRT (Fig. S2).

480

481 [Fig. S3](#) illustrates the concentration profiles of acetate and CH₄ over time in SBR operated at
482 four different acetate concentration under 50 days SRT. At all concentration, acetate was
483 rapidly depleted after each feeding cycle, with the simultaneous methane production. At higher
484 organic concentrations (3 and 5 g COD/L), acetate exhibited pronounced periodic fluctuations,
485 while CH₄ production reached saturation early. The Gibbs free energy profiles revealed that
486 under low acetate concentrations (e.g., 0.2 g COD/L), ΔG values remained more negative
487 (approaching -10 kJ/mol) compared to those at higher concentrations (e.g., -3 kJ/mol at 5 g
488 COD/L), probably indicating more thermodynamically favorable conditions for acetoclastic
489 methanogenesis. These low available energy conditions probably advantageous for
490 *Methanotrix* over *Methanosarcina*, thereby might explain its competitive dominance under
491 low substrate concentration. [Fig. S4](#) illustrates the concentration details of acetate and CH₄ in
492 CFR operated at different acetate concentration under 50 days SRT. Acetate remained
493 consistently low (< 0.1 g COD/L) across all influent COD concentrations, while increasing
494 COD accelerated methane production. Methane production initially increases due to system
495 startup, then stabilizes once the system reaches a steady state. At all influent COD
496 concentrations, ΔG stabilized below -30 kJ/mol after the initial stage, indicating consistently
497 favorable thermodynamic conditions for methanogenesis. The more negative ΔG values
498 observed at higher COD levels reflect greater energy yield, which might favor *Methanosarcina*,
499 as a competitive acetoclastic methanogen under energy-rich conditions. While lower acetate
500 concentrations with lower available energy might create an optimal niche for *Methanotrix*.

501

502 In summary, as the acetate concentration increases, *Methanotrix* requires longer SRTs to
503 achieve dominance. Under high organic concentration conditions, *Methanosarcina* rapidly
504 accumulates in the early stages due to its high maximum growth rate and tolerance to substrate

505 fluctuations. However, as the SRT increases, its population may decline, possibly because it is
506 less adapted to densely populated environments. *Methanosarcina* has a faster growth rate and
507 efficiently utilizes substrate under short SRTs, whereas *Methanothrix*, though slower growing,
508 exhibits a stable and robust enrichment trend under prolonged SRTs. This aligns with classical
509 chemostat theory, which predicts that slower-growing organisms are excluded at high dilution
510 rates, but can outcompete faster growers under low dilution rates. The dominance of
511 *Methanosarcina* under short SRTs or high loading rates (e.g., in high-rate UASB reactors)
512 (Zhang et al., 2020) reflects the predictions of classical chemostat models regarding r-
513 strategists. Conversely, the shift toward *Methanothrix* under extended SRTs demonstrates a
514 typical K-strategist behavior. In anaerobic systems with long SRTs or stable operation (e.g.,
515 fixed-bed or membrane bioreactors), *Methanothrix* demonstrated better adaptability and
516 contributes to long-term system stability (Hou et al., 2020). In these systems, biomass is
517 retained via biofilm attachment or membrane separation, preventing microbial washout and
518 thereby altering competition dynamics relative to those in CFRs or SBRs. One deviation from
519 classical chemostat theory is the observed coexistence of *Methanosarcina* and *Methanothrix* at
520 long SRTs in SBRs, which may be attributed to the long-term retention of *Methanothrix* near
521 its critical SRT, even over a decade, an effect not captured by idealized steady-state models.

522

523 **3.6. Effect of acetate concentration on the selection of r-/K-strategists**

524 The contour plots (Fig. 6) illustrate the distinct biomass accumulation patterns of *Methanothrix*
525 and *Methanosarcina* in SBR and CFR under varying acetate concentrations. *Methanothrix*
526 showed a clear preference for low acetate concentrations (0.2 ~ 0.5 g COD/L) and long SRTs
527 (> 35 days) in SBR, reaching a peak biomass concentration of approximately 0.31 g COD/L at
528 an SRT of 50 days (Fig. 6b). Its biomass increased steadily with SRT but declined as acetate
529 concentration exceeded 0.5 g COD/L, indicating its adaptation to substrate-limited conditions

530 (Chang et al., 2024; De Vrieze et al., 2012). According to the study of Straub et al. (2006),
531 *Methanosarcina* demonstrated a competitive dominance over *Methanothrix* when acetate
532 concentrations above 0.14 g COD/L. *Methanosarcina* exhibited a rapid initial biomass increase
533 at high acetate concentrations (> 3 g COD/L) at short SRTs, suggesting its preference for high
534 substrate availability. This suggests a strong tolerance to high substrate concentration and fast
535 growth under favorable substrate conditions for *Methanosarcina*. However, at low acetate
536 concentrations (< 0.2 g COD/L), the abundance of *Methanosarcina* remained minimal,
537 suggesting its limited competitiveness under substrate-limited conditions (Conklin et al., 2006).
538 These findings highlight the distinct ecological strategies of the two methanogens:
539 *Methanothrix*, a K-strategist, dominates in stable, low-substrate environments, whereas
540 *Methanosarcina*, an r-strategist, excels under high substrate concentration (Straub et al., 2006).
541
542 The abundance trend of *Methanosarcina* in the CFR closely mirrored that in the SBR, showing
543 a consistent response to acetate concentration across both systems (Fig. 6c). In contrast, CFR
544 systems showed a more pronounced shift in microbial dominance with acetate concentration
545 increase for *Methanothrix* (Fig. 6d). *Methanothrix* biomass increased steadily with acetate
546 concentration decrease, peaking at 0.46 g COD/L biomass at 2.5 g COD/L under 50 days SRT.
547 It also maintained moderate biomass under low acetate conditions (0.2 ~ 1.0 g COD/L),
548 reinforcing its high substrate affinity and competitive fitness in continuous systems. This shift
549 indicates that CFR systems, which maintain stable flow and minimize substrate fluctuations,
550 favor the enrichment of *Methanothrix* over time (Chang et al., 2025). This differential
551 ecological adaptation has important implications for the targeted enrichment of acetoclastic
552 methanogens in anaerobic digestion processes, depending on system configuration and
553 operational goals.

554

555 **4. Conclusions**

556 The thermodynamic energy dissipation approach combined with metabolic energy analysis
557 offers a promising framework for differentiating the kinetic characteristics of the two
558 methanogens. The observed kinetic diversity among functional microorganisms in anaerobic
559 digestion highlights the relevance of incorporating r/K selection theory into ADMMs. Targeted
560 manipulation of r- and K-strategists, individually or in combination, can be realized by
561 adjusting operational parameters such as operational mode, solid retention time, and acetate
562 concentration. Sensitivity analysis revealed that *Methanosarcina* was strongly affected by
563 biomass yield and acetate concentration, while the enrichment of *Methanothrix* could be
564 effectively controlled by adjusting SRT. *Methanosarcina* showed a higher biomass yield under
565 high acetate concentration, whereas *Methanothrix* demonstrated a sustained enrichment trend
566 under extended SRTs or low substrate concentrations in CFRs.

567

568 **Acknowledgements**

569 This study was supported by the Taighde Éireann – Research Ireland (formerly Science
570 Foundation Ireland) and the Sustainable Energy Authority of Ireland under the SFI Frontiers
571 for the Future Awards Programme (22/FFP-A/10346). Huanhuan Chang thanks the scholarship
572 from the China Scholarship Council (No. 202208620052). Guangxue Wu thanks the support
573 from the Galway University Foundation.

574

575 **References**

576 Aguilar-Muñoz, P., Lavergne, C., Chamy, R., Cabrol, L., 2022. The biotechnological potential
577 of microbial communities from Antarctic soils and sediments: Application to low
578 temperature biogenic methane production. *J. Biotechnol.* 351, 38-49.
579 Andrews, J.H., Harris, R.F., 1986. r- and K-Selection and Microbial Ecology. *Advances in*

580 Microbial Ecology. (Ed.) K.C. Marshall. Springer US, Boston, MA, pp. 99-147.

581 Batstone, D.J., Keller, J., 2003. Industrial applications of the IWA anaerobic digestion model
582 No. 1 (ADM1). Water Sci. Technol. 47 (12), 199-206.

583 Batstone, D.J., Keller, J., Angelidaki, I., Kalyuzhnyi, S.V., Pavlostathis, S.G., Rozzi, A.,
584 Sanders, W., Siegrist, H., Vavilin, V.A., 2002. The IWA anaerobic digestion model no 1
585 (ADM1). Water Sci. Technol. 45 (10), 65-73.

586 Bonk, F., Popp, D., Weinrich, S., Sträuber, H., Becker, D., Kleinstaub, S., Harms, H., Centler,
587 F., 2019. Determination of microbial maintenance in acetogenesis and methanogenesis by
588 experimental and modeling techniques. Front. Microbiol. 10, 166.

589 Boone David, R., Johnson Richard, L., Liu, Y., 1989. Diffusion of the interspecies electron
590 carriers H₂ and formate in methanogenic ecosystems and its implications in the
591 measurement of K_m for H₂ or formate uptake. Appl. Environ. Microbiol. 55 (7), 1735-1741.

592 Buan, N.R., 2018. Methanogens: pushing the boundaries of biology. Emerging Top. Life Sci. 2
593 (4), 629-646.

594 Chang, H., Du, B., He, K., Yin, Q., Wu, G., 2024. Mechanistic understanding of acclimation
595 and energy metabolism of acetoclastic methanogens under different substrate to
596 microorganism ratios. Environ. Res. 252, 118911.

597 Chang, H., Yin, Q., He, K., De Vrieze, J., Wu, G., 2025. Feeding regime selectively enriching
598 acetoclastic methanogens to enhance energy production in anaerobic digestion systems.
599 Biochem. Eng. J. 220, 109764.

600 Chen, X., Chen, Z., Wang, X., Huo, C., Hu, Z., Xiao, B., Hu, M., 2016. Application of ADM1
601 for modeling of biogas production from anaerobic digestion of *Hydrilla verticillata*.
602 Bioresour. Technol. 211, 101-107.

603 Conklin, A., Stensel, H.D., Ferguson, J., 2006. Growth Kinetics and Competition Between
604 *Methanosarcina* and *Methanosaeta* in Mesophilic Anaerobic Digestion. Water Environ.

605 Res 78 (5), 486-496.

606 Couto, P.T., Brustello, M., Albanez, R., Rodrigues, J.A.D., Zaiat, M., Ribeiro, R., 2019.
607 Calibration of ADM1 using the Monte Carlo Markov Chain for modeling of anaerobic
608 biodigestion of sugarcane vinasse in an AnSBBR. Chem. Eng. Res. Des. 141, 425-435.

609 De Vrieze, J., Hennebel, T., Boon, N., Verstraete, W., 2012. *Methanosarcina*: The rediscovered
610 methanogen for heavy duty biomethanation. Bioresour. Technol. 112, 1-9.

611 Delattre, H., Chen, J., Wade, M.J., Soyer, O.S., 2020. Thermodynamic modelling of synthetic
612 communities predicts minimum free energy requirements for sulfate reduction and
613 methanogenesis. J. R. Soc. Interface 17 (166), 20200053.

614 Duan, X., Luo, J., Su, Y., Liu, C., Feng, L., Chen, Y., 2023. Proteomic profiling of robust
615 acetoclastic methanogen in chrysene-altered anaerobic digestion: Global dissection of
616 enzymes. Water Res. 233, 119817.

617 Figdore, B., Yilmaz, V., Yilmazel, Y.D., Duran, M., 2013. Modeling competition among
618 acetoclastic methanogenic species during anaerobic digestion of municipal biosolids. Ecol.
619 Urban Areas, 202.

620 Havlik, I., Votruba, J., Sobotka, M., Volesky, B., 1984. Parametric sensitivity in modeling of
621 anaerobic digestion. Biotechnol. Lett. 6 (9), 607-610.

622 Heijnen, J.J., 2002. Bioenergetics of microbial growth. Encyclopedia of Bioprocess Technology.
623 John Wiley & Sons, New York, pp. 267-291.

624 Heijnen, J.J., Kleerebezem, R., 2010. Bioenergetics of microbial growth. Encyclopedia of
625 Industrial Biotechnology: Bioprocess, Bioseparation and Cell Technology. John Wiley &
626 Sons, New York, pp. 594-617.

627 Heijnen, J.J., Van Dijken, J.P., 1992. In search of a thermodynamic description of biomass
628 yields for the chemotrophic growth of microorganisms. Biotechnol. Bioeng. 39 (8), 833-
629 858.

630 Hou, L., Griswold, N., Hu, Z., 2020. Impact of decreasing hydraulic retention times on the
631 specific affinity of methanogens and their community structures in an anaerobic membrane
632 bioreactor process treating low strength wastewater. *Sci. Total Environ.* 739, 140373.

633 Jetten, M.S.M., Stams, A.J.M., Zehnder, A.J.B., 1990. Acetate threshold values and acetate
634 activating enzymes in methanogenic bacteria. *FEMS Microbiol. Lett.* 73 (4), 339-344.

635 Jin, Q., 2012. Energy conservation of anaerobic respiration. *Am. J. Sci.* 312 (6), 573-628.

636 Kleerebezem, R., and Van Loosdrecht, M.C.M., 2010. A Generalized Method for
637 Thermodynamic State Analysis of Environmental Systems. *Crit. Rev. Environ. Sci.*
638 *Technol.* 40 (1), 1-54.

639 Kleerebezem, R., van Loosdrecht, M.C., 2006. Critical analysis of some concepts proposed in
640 ADM1. *Water Sci. Technol.* 54 (4), 51-57.

641 Lee, E., Min, K.J., Park, K.Y., 2025. Changes in anaerobic digestion performance and microbial
642 community by increasing SRT through sludge recycling in food waste leachate treatment.
643 *Sci. Rep.* 15 (1), 19845.

644 Leurent, A., Moscoviz, R., 2022. Modeling a propionate-oxidizing syntrophic coculture using
645 thermodynamic principles. *Biotechnol. Bioeng.* 119 (9), 2423-2436.

646 Liu, T., Wu, G., 2023. Mathematical model of anaerobic propionate degradation by
647 incorporating the r/K selection theory. *J. Water Process Eng.* 56, 104488.

648 López, I., Borzacconi, L., 2010. Modelling of slaughterhouse solid waste anaerobic digestion:
649 Determination of parameters and continuous reactor simulation. *Waste Manage.* 30 (10),
650 1813-1821.

651 Lv, W., Zhang, W., Yu, Z., 2016. Volume ratios between the thermophilic and the mesophilic
652 digesters of a temperature-phased anaerobic digestion system affect their performance and
653 microbial communities. *New Biotechnol.* 33 (1), 245-254.

654 Melcer, H., 2004. Methods for wastewater characterization in activated sludge modelling. IWA

655 publishing.

656 Merkel, W., Krauth, K., 1999. Mass transfer of carbon dioxide in anaerobic reactors under
657 dynamic substrate loading conditions. *Water Res.* 33 (9), 2011-2020.

658 Mo, R., Guo, W., Batstone, D., Makinia, J., Li, Y., 2023. Modifications to the anaerobic
659 digestion model no. 1 (ADM1) for enhanced understanding and application of the
660 anaerobic treatment processes - A comprehensive review. *Water Res.* 244, 120504.

661 Pan, X., Zhao, L., Li, C., Angelidaki, I., Lv, N., Ning, J., Cai, G., Zhu, G., 2021. Deep insights
662 into the network of acetate metabolism in anaerobic digestion: focusing on syntrophic
663 acetate oxidation and homoacetogenesis. *Water Res.* 190, 116774.

664 Patón, M., Rodríguez, J., 2019. A compilation and bioenergetic evaluation of syntrophic
665 microbial growth yields in anaerobic digestion. *Water Res.* 159, 176-183.

666 Picioreanu, C., Head, I.M., Katuri, K.P., van Loosdrecht, M.C.M., Scott, K., 2007. A
667 computational model for biofilm-based microbial fuel cells. *Water Res.* 41 (13), 2921-
668 2940.

669 Reichert, P., 1994. AQUASIM-A tool for simulation and data analysis of aquatic systems. *Water*
670 *Sci. Technol.* 30 (2), 21-30.

671 Reichert, P., 1998. Aquasim 2.0-user manual. Swiss Federal Institute for Environmental Science
672 and Technology. Dübendorf, Switzerland.

673 Rittmann, B.E., McCarty, P.L., 2020. *Environmental biotechnology: principles and applications.*
674 Second edition ed. McGraw-Hill Education, New York.

675 Salma, A., Laferte, J.M., Fryda, L., Djelal, H., 2025. Advancing Bioenergy: In-situ and in-silico
676 Approach To Enhance Anaerobic Digestion. *Waste Biomass Valori.*

677 Sani, K., O-Thong, S., Jariyaboon, R., Reungsang, A., Yasui, H., Kongjan, P., 2025. Anaerobic
678 co-digestion of glycerol waste and distillery wastewater for bio-hythane production:
679 Performance and ADM-1 based kinetics. *Carbon Resour. Convers.* 8 (3), 100311.

680 Schmidt, J.E., Ahring, B.K., 1999. Immobilization patterns and dynamics of acetate-utilizing
681 methanogens immobilized in sterile granular sludge in upflow anaerobic sludge blanket
682 reactors. *Appl. Environ. Microbiol.* 65 (3), 1050-1054.

683 Segura, T., Zanoni, P., Brémond, U., Lucet--Bérille, C., Pradel, A., Escudié, R., Steyer, J.-P.,
684 2025. Modelling anaerobic digestion of agricultural waste: From lab to full scale. *Waste*
685 *Manage.* 200, 114739.

686 Siegrist, H., Vogt, D., Garcia-Heras, J.L., Gujer, W., 2002. Mathematical model for meso- and
687 thermophilic anaerobic sewage sludge digestion. *Environ. Sci. Technol.* 36 (5), 1113-1123.

688 Silva, T.P., Silva Júnior, F.d.C.G.d., Gehring, T.A., de Menezes, C.A., Almeida, P.d.S., Zaiat,
689 M., dos Santos, A.B., Leitão, R.C., 2025. Anaerobic Digestion Model No. 1 applied to
690 bioenergy generation from fruit and vegetable waste in Upflow Anaerobic Sludge Blanket
691 reactors. *Bioresour. Technol.* 432, 132644.

692 Straub, A., Conklin, A., Ferguson, J., Stensel, H., 2006. Use of the ADM1 to investigate the
693 effects of acetoclastic methanogen population dynamics on mesophilic digester stability.
694 *Water Sci. Technol.* 54 (4), 59-66.

695 Sun, H., Yang, Z., Shi, G., Arhin, S.G., Papadakis, V.G., Goula, M.A., Zhou, L., Zhang, Y., Liu,
696 G., Wang, W., 2021a. Methane production from acetate, formate and H₂/CO₂ under high
697 ammonia level: Modified ADM1 simulation and microbial characterization. *Sci. Total*
698 *Environ.* 783, 147581.

699 Sun, H., Yang, Z., Zhao, Q., Kurbonova, M., Zhang, R., Liu, G., Wang, W., 2021b. Modification
700 and extension of anaerobic digestion model No.1 (ADM1) for syngas biomethanation
701 simulation: From lab-scale to pilot-scale. *Chem. Eng. J.* 403, 126177.

702 Tijhuis, L., Van Loosdrecht, M.C.M., Heijnen, J.J., 1993. A thermodynamically based
703 correlation for maintenance gibbs energy requirements in aerobic and anaerobic
704 chemotrophic growth. *Biotechnol. Bioeng.* 42 (4), 509-519.

705 von Stockar, U., 2014. Optimal energy dissipation in growing microorganisms and rectification
706 columns. *J. Non-Equilib. Thermodyn.* 39 (1), 3-11.

707 Wandrey, C., Aivasidis, A., 1983. Continuous anaerobic digestion with *Methanosarcina barkeri*.
708 *Ann. N. Y. Acad. Sci.* 413 (1), 489-500.

709 Welte, C., Deppenmeier, U., 2014. Bioenergetics and anaerobic respiratory chains of
710 acetoclastic methanogens. *Biochim. Biophys. Acta* 1837 (7), 1130-1147.

711 Wu, Q., Guthrie, M.J., Jin, Q., 2022. Physiological acclimation extrapolates the kinetics and
712 thermodynamics of methanogenesis from laboratory experiments to natural environments.
713 *Front. Ecol. Evol.* 10, 838487.

714 Yin, Q., Sun, Y., Li, B., Feng, Z., Wu, G., 2022. The r/K selection theory and its application in
715 biological wastewater treatment processes. *Sci. Total Environ.* 824, 153836.

716 Zhang, L., Guo, B., Mou, A., Li, R., Liu, Y., 2020. Blackwater biomethane recovery using a
717 thermophilic upflow anaerobic sludge blanket reactor: Impacts of effluent recirculation on
718 reactor performance. *J. Environ. Manage.* 274, 111157.

719 Zhao, X., Li, L., Wu, D., Xiao, T., Ma, Y., Peng, X., 2019. Modified Anaerobic Digestion Model
720 No. 1 for modeling methane production from food waste in batch and semi-continuous
721 anaerobic digestions. *Bioresour. Technol.* 271, 109-117.

722 Zhu, X., Ji, Y., Huang, Q., Shen, W., Wei, Z., Ma, J., Zhang, G., Xu, H., 2024. Temporal
723 variation of methanogenic pathways in rice fields under three different cropping systems.
724 *Biol. Fertility Soils* 60 (6), 743-756.

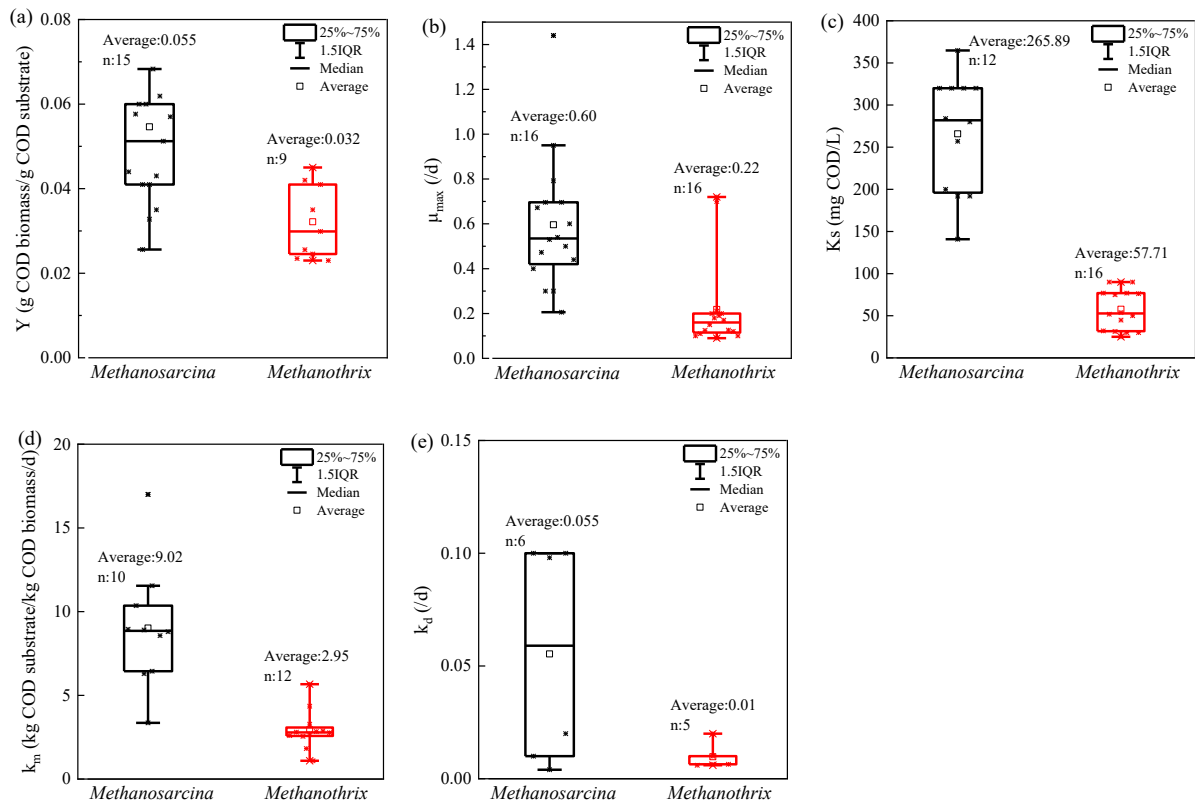


Fig. 1. Kinetic parameters of *Methanosarcina* and *Methanothrix*, (a) biomass yield (Y); (b) maximum specific growth rate (μ_{max}); (c) half-saturation constant (K_s); (d) maximum specific substrate utilization rate (k_m); (e) decay rate (k_d).

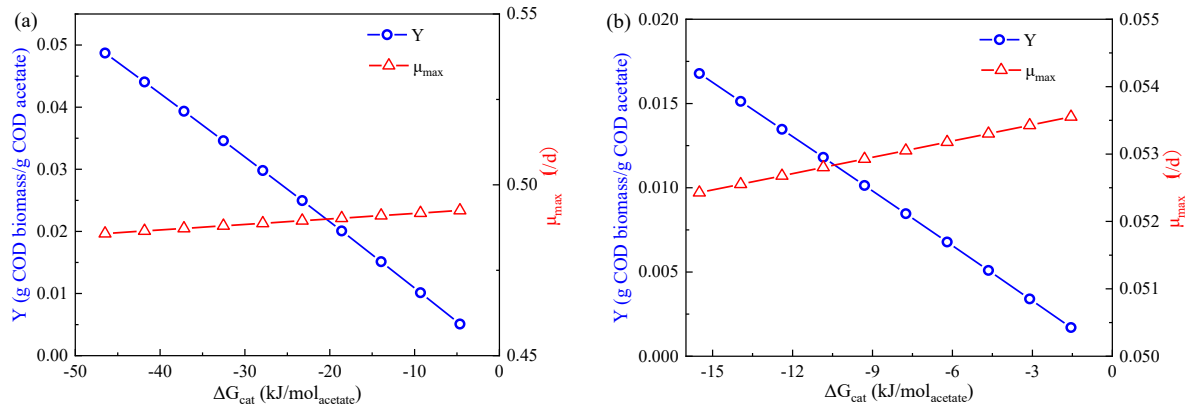


Fig. 2. Kinetic parameter (Y and μ_{max}) estimation of (a) *Methanosarcina* and (b) *Methanotrix* based on thermodynamic dissipation.

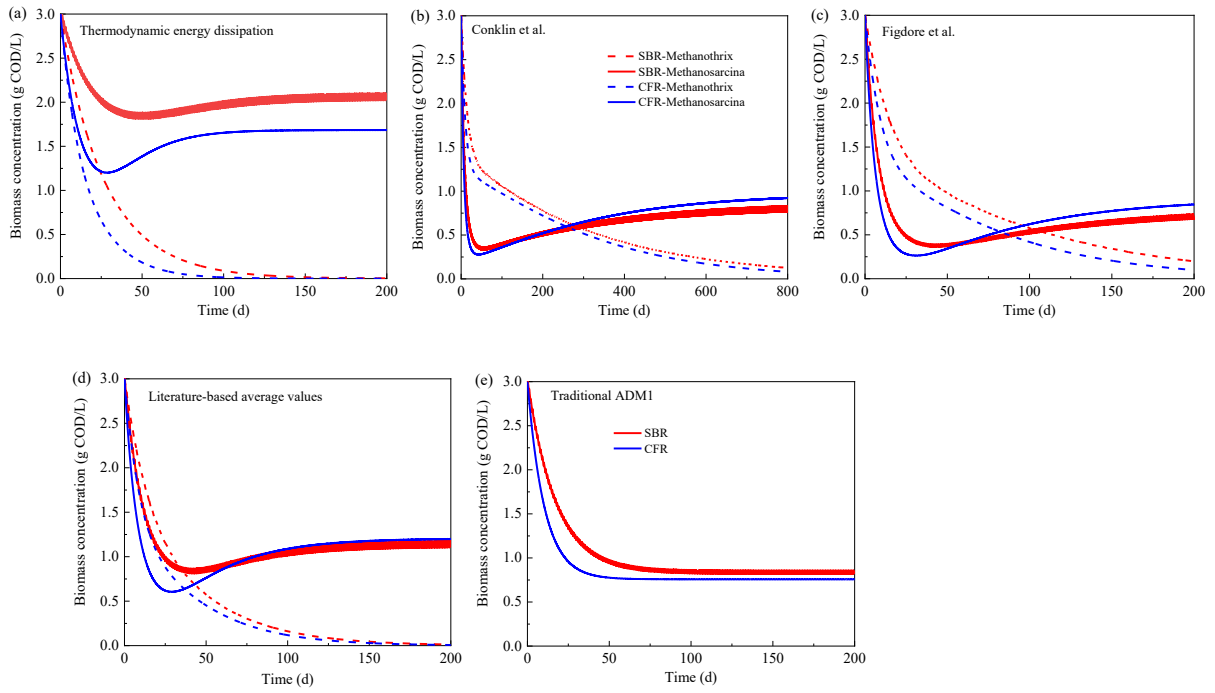


Fig. 3. Simulation results based on different data sources: (a) thermodynamic energy dissipation results; (b) experimental data from Conklin et al.; (c) model data from Figdore et al.; (d) literature-based average values; (e) data from traditional ADM1 model.

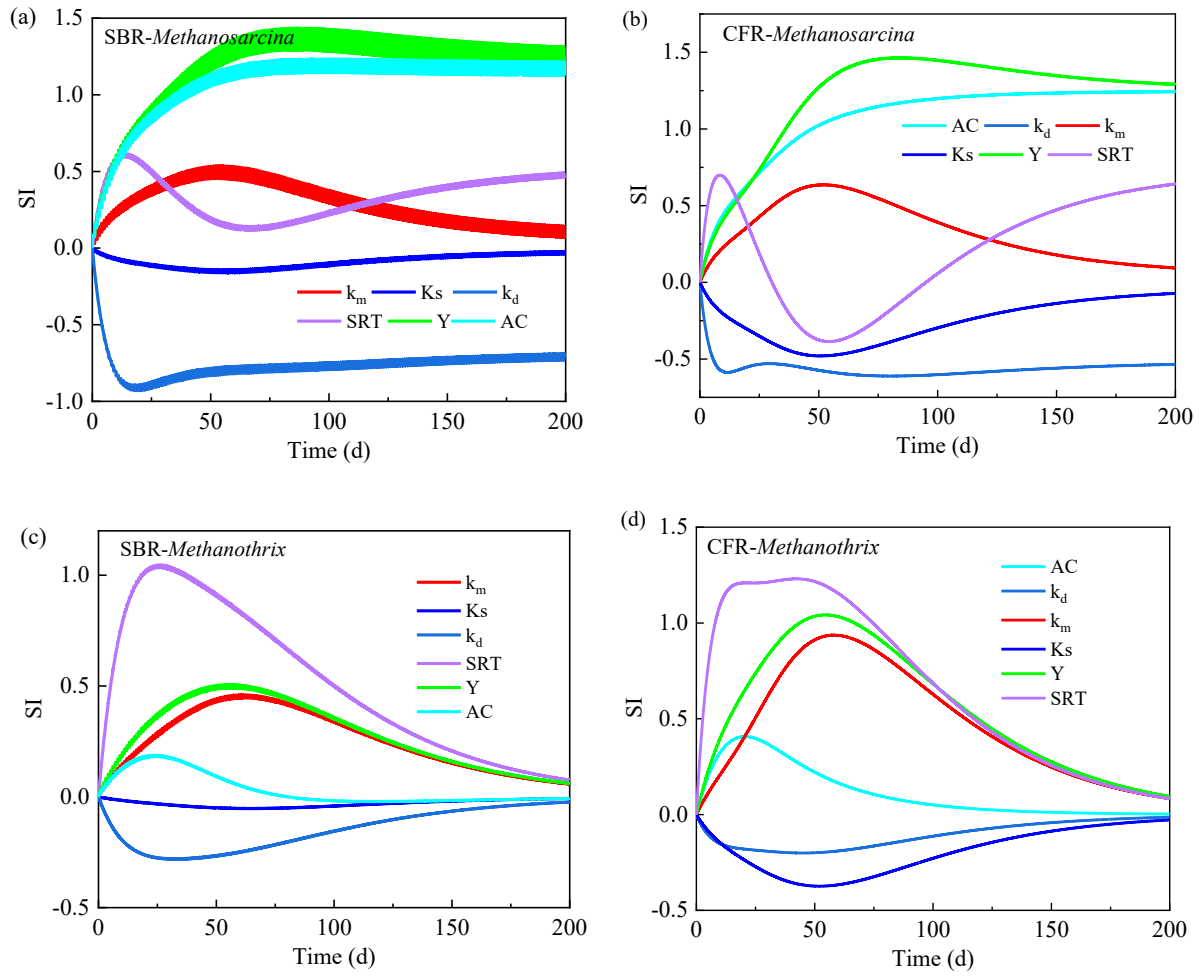


Fig. 4. Sensitivity analysis of k_m , k_d , K_s , Y , SRT, and acetate concentration (AC) for *Methanosarcina* in (a) SBR and (b) CFR, and for *Methanothrix* in (c) SBR and (d) CFR.

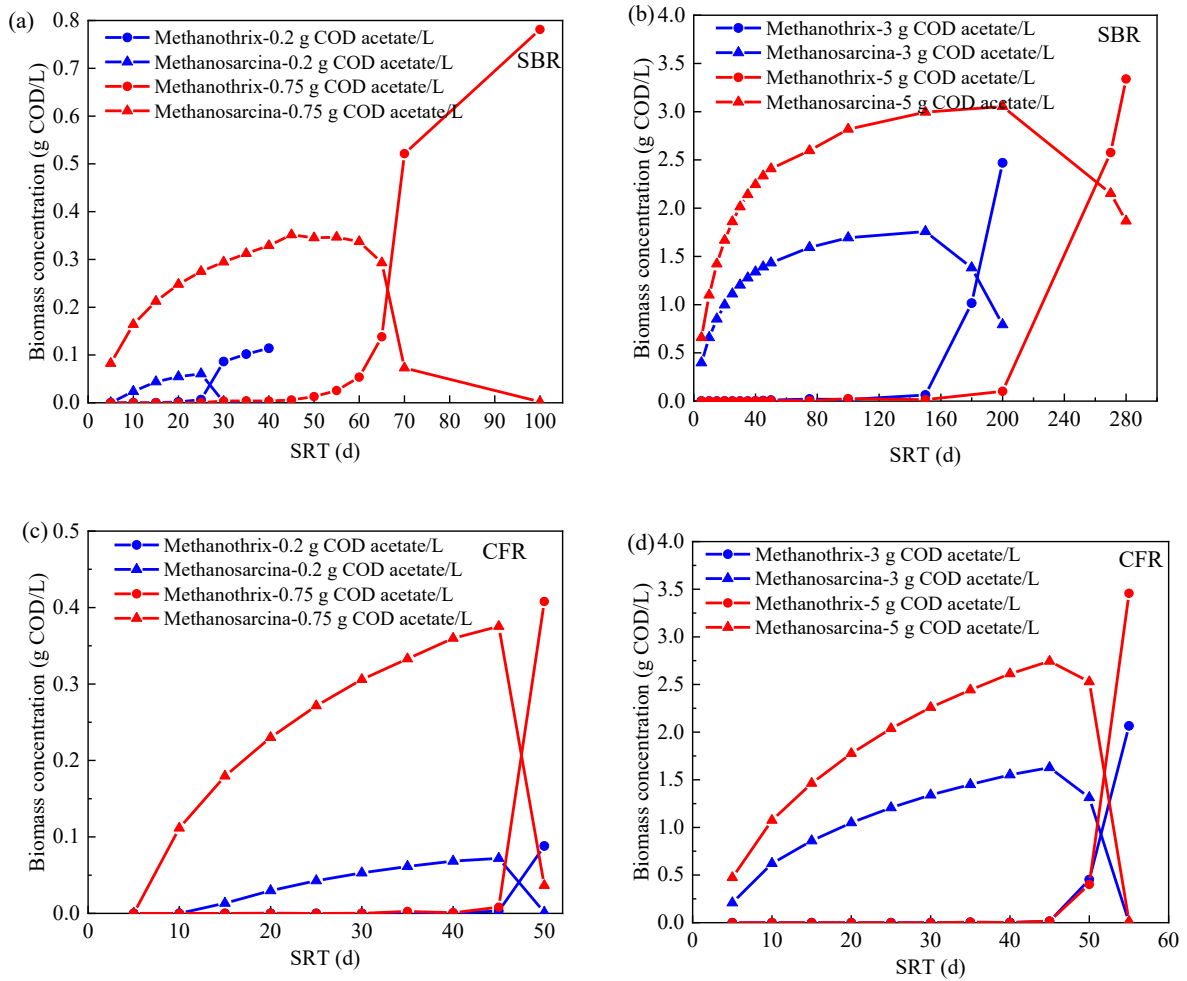


Fig. 5. Effect of SRT on the competition between *Methanosarcina* and *Methanothrix* in (a, b) SBR and (c, d) CFR systems under varying acetate concentrations: 0.2, 0.75, 3, and 5 g COD/L.

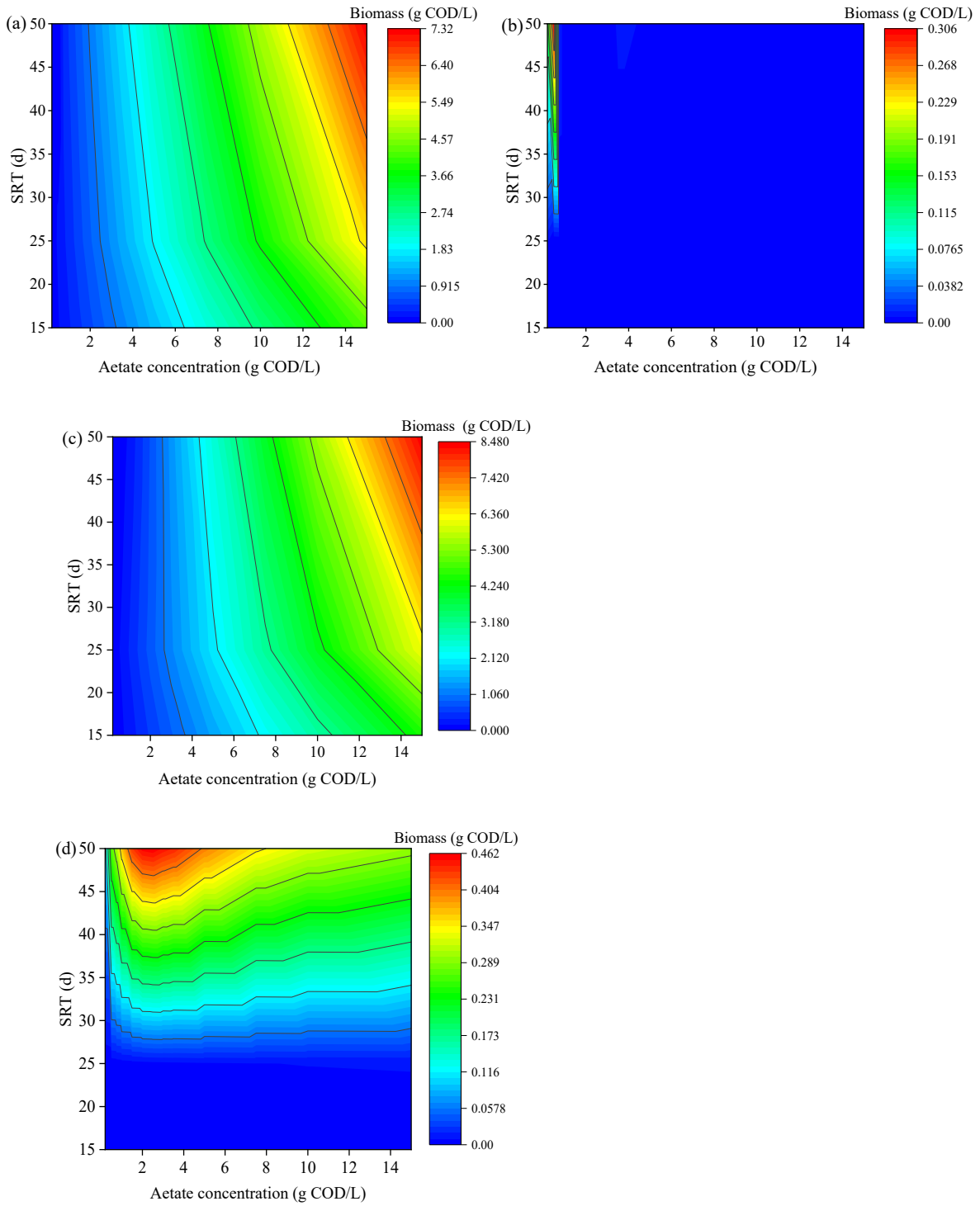


Fig. 6. Effect of acetate concentration on the biomass concentration of (a) *Methanosarcina* and (b) *Methanothrix* in SBR, and (c) *Methanosarcina* and (d) *Methanothrix* in CFR.